Eur. Phys. J. B **22**, 249–256 (2001)

THE EUROPEAN PHYSICAL JOURNAL B

EDP Sciences

Linear and nonlinear optical properties of semiconductor nanorings with magnetic field and disorder – Influence on excitons and biexcitons

T. Meier[a], P. Thomas, and S.W. Koch

Department of Physics and Material Sciences Center, Philipps University, Renthof 5, 35032 Marburg, Germany

Received 31 January 2001

Abstract. Linear and nonlinear optical absorption spectra are studied theoretically for semiconductor nanorings penetrated by a magnetic field. Due to the Aharanov-Bohm effect the spectral position as well as the oscillator strength of the exciton change periodically as function of the magnetic flux enclosed by the ring. In the nonlinear differential absorption spectra it is found that the magnetic field strongly modifies Coulomb many-body correlations. In particular, the magnetic-field-induced increase of the exciton binding energy is accompanied by a decrease of the biexciton binding energy. The persistence of these effects in the presence of energetic disorder is analyzed.

PACS. 71.35.Cc Intrinsic properties of excitons; optical absorption spectra – 78.66.-w Optical properties of specific thin films – 42.50.Md Optical transient phenomena: quantum beats, photon echo, free-induction decay, dephasings and revivals, optical nutation, and self-induced transparency – 03.65.Bz Foundations, theory of measurement, miscellaneous theories

1 Introduction

During the past two decades optical properties of semiconductor nanostructures with reduced dimensionality have been investigated in numerous experimental and theoretical studies. Such systems are highly interesting from the fundamental point of view, since they offer ways of studying, for example, interaction processes in reduced dimension. Furthermore, due to the possibility of designing the optical and electronic properties they are important for many applications. In particular, magnetic-field-induced effects in ring-like semiconductor nanostructures have attracted some attention [1–3]. The optical properties of such semiconductor nanorings were investigated experimentally by infrared spectroscopy which probes intraband and intersubband transitions [3]. Also the interband photoluminescence of charged rings [4] and the exciton absorption [5] have been studied.

In this paper we present a theoretical approach and numerical results for a simple model system which allows us to investigate the linear and, in particular, nonlinear optical properties of interband transitions in semiconductor nanorings with magnetic field and disorder. For narrow ordered rings we reproduce the findings of references [6] and [7] which showed that in the linear absorption spectra the spectral position of the exciton as well as its oscillator strength change periodically with the magnetic flux Φ enclosed by the ring. The period of these oscillations is given by the flux quantum $\Phi_0 = hc/e$.

We compute nonlinear pump-probe spectra for counter-clockwise polarized pulses and predict that the magnetic field strongly influences Coulombic many-particle correlations. In this geometry the differential absorption spectra of ordered systems are purely induced by many-body correlations as long as only heavy-hole and no light-hole transitions are relevant [8–11]. In particular, it is shown that the binding energy of the bound biexciton changes as function of Φ. For $\Phi/\Phi_0 = 0.5$ it is smaller than without magnetic field, whereas the exciton binding energy behaves the opposite way. The origin of the magnetic-field-induced modifications of the spectral positions of bound and unbound biexcitons is discussed. Our findings demonstrate that the Aharanov-Bohm effect [12] does influence quasiparticles like excitons and biexcitons and that it should be possible to investigate such effects using optical interband spectroscopy.

As realistic nanostructures exhibit some structural disorder on mesoscopic scales we study the influence of energetic disorder on the magnetic-field-induced changes of the linear and nonlinear absorption spectra. It is shown that the excitonic shift survives in the presence of energetic disorder, even when the disorder-induced inhomogeneous broadening of the absorption lines exceeds the magnetic-field-induced shift of the exciton line. Furthermore, we show and discuss results on linear and nonlinear optical spectra of single disordered rings.

We start in Section 2 by introducing our theoretical approach. The action of the magnetic field in the ring is discussed in Section 2.1. The equations of motion that are used to describe nonlinear optical processes including

[a] e-mail: torsten.meier@physik.uni-marburg.de

many-body correlations within the coherent third-order ($\chi^{(3)}$) limit are derived and discussed in Section 2.2. This extends our previous analysis of the coherent dynamics of magnetoexcitons [13] by including interacting two-exciton states, which are known to strongly influence the optical response already in the $\chi^{(3)}$ limit. Details on the model system used here are given in Section 2.3. Numerical results on linear and nonlinear optical spectra are presented and analyzed in Section 3. We first focus on the ordered case in Section 3.1 and then include energetic disorder in Section 3.2. The paper closes with a brief summary in Section 4.

2 Theoretical approach

2.1 Magnetic field in ring geometry

To model a ring we use a finite number of equidistantly spaced sites (N) and apply periodic boundary conditions. Each localized site carries states with energies ϵ_n^c and ϵ_n^v which due to the coupling between the sites give rise to the conduction and valence bands. In our finite and discrete model system the electronic couplings of the respective bands are described by a matrices T_{nm}^c and T_{nm}^v [13]. The energies ϵ_n^c and ϵ_n^v are the diagonal elements T_{nn}^c and T_{nn}^v. In the absence of disorder they are taken as half the transition energy of a single site, *i.e.* $T_{nn}^c = E_g/2$ (for the holes we use $T_{nn}^v = E_g/2$). The inclusion of energetic disorder is discussed in Section 3.2.

The nondiagonal matrix elements of T define the couplings between of the localized basis states. Within the tight-binding approximation the only nonvanishing off-diagonal elements are $T_{n,n+1}^c$ and $T_{n+1,n}^c$. In the absence of a magnetic field the coupling is independent of the direction, *i.e.* $T_{n,n+1}^c = T_{n+1,n}^c = J_c$ and $T_{n,n+1}^v = T_{n+1,n}^v = J_v$.

In the presence of a magnetic field the nearest-neighbour coupling is given by [13]

$$\begin{aligned} T_{n,n+1}^c &= J_c \exp[\mathrm{i}2\pi(\Phi/N)/\Phi_0]\,, \\ T_{n+1,n}^c &= J_c \exp[-\mathrm{i}2\pi(\Phi/N)/\Phi_0] \end{aligned} \tag{1}$$

for the conduction band. Accordingly, the positively charged holes in the valence band are described by

$$\begin{aligned} T_{n,n+1}^v &= J_v \exp[-\mathrm{i}2\pi(\Phi/N)/\Phi_0]\,, \\ T_{n+1,n}^v &= J_v \exp[\mathrm{i}2\pi(\Phi/N)/\Phi_0]\,. \end{aligned} \tag{2}$$

Compared to the case without magnetic field, the tight-binding coupling parameters J_c and J_v are thus multiplied by a phase factor which depends on the magnetic flux Φ through the ring [14,15]. $\Phi_0 = hc/e$ is the flux quantum.

One can easily see how the magnetic field acts in reciprocal space. Without magnetic field and disorder the eigenfunctions of the tight-binding model are plane waves, *i.e.*

$$\Psi_k(n) = (1/\sqrt{N}) \exp[\mathrm{i}knd]\,, \tag{3}$$

where n is an integer and d is the distance between the sites. The energies follow a cosine dispersion $-2J\cos[kd]$ and the allowed values for the wavevector are quantized and can be chosen as

$$k = -\frac{2\pi}{d}\frac{\frac{N}{2}-1}{N}, -\frac{2\pi}{d}\frac{\frac{N}{2}-2}{N}, ..., \frac{2\pi}{d}\frac{\frac{N}{2}}{N}\,. \tag{4}$$

With magnetic field the flux-dependent phase factor must be taken into account and we thus have

$$\begin{aligned} k = &-\frac{2\pi}{d}\frac{\frac{N}{2}-1-\Phi/\Phi_0}{N}, -\frac{2\pi}{d}\frac{\frac{N}{2}-2-\Phi/\Phi_0}{N}, ..., \\ &\frac{2\pi}{d}\frac{\frac{N}{2}-\Phi/\Phi_0}{N}\,. \end{aligned} \tag{5}$$

Thus the allowed values for the wavevector are simply shifted by a constant value that is proportional to the flux [14,16].

2.2 Equations of motion including many-body correlations

To calculate optical properties of semiconductor nanorings we use the same approach as described in references [9,17]. We express the nonlinear optical response using the so-called dynamics-controlled truncation scheme up to the coherent $\chi^{(3)}$-limit [18,19]. In this limit the optical response can be fully expressed by correlation functions describing excitation of single and two electron-hole-pairs, *i.e.* exciton and biexciton amplitudes.

We start from the general Hamiltonian [20]:

$$H = H_0 + H_\mathrm{C} + H_\mathrm{I}, \tag{6}$$

where H_0 is the single-particle Hamiltonian, H_C describes the Coulomb interaction, and H_I the interaction with a classical electric field.

Using second quantization the single-particle Hamiltonian H_0 reads in a localized real-space basis:

$$H_0 = \sum_{nmc} T_{nm}^c c_n^{c+} c_m^c + \sum_{nmv} T_{nm}^v d_n^{v+} d_m^v. \tag{7}$$

Here, c_n^{c+} (c_m^c) creates (destroys) an electron at site n (m) in band c and d_n^{v+} (d_m^v) creates (destroys) a hole at site n (m) in band v.

The Coulomb Hamiltonian H_C is used as:

$$H_\mathrm{C} = \frac{1}{2}\sum_{nm\nu\nu'} (c_n^{\nu+} c_n^\nu - d_n^{\nu+} d_n^\nu) V_{nm} (c_m^{\nu'+} c_m^{\nu'} - d_m^{\nu'+} d_m^{\nu'}), \tag{8}$$

where V_{nm} describes the monopole-monopole Coulomb interaction between particles at sites n and m and the superscripts ν and ν' label the relevant valence and conduction bands. H_C includes the repulsion between electrons and between holes, as well as the electron-hole attraction.

The coupling of the electronic system to a classical electric field is described by:

$$\begin{aligned} H_\mathrm{I} &= -\mathbf{E}(t)\cdot\mathbf{P} \\ &= -\mathbf{E}(t)\cdot\sum_{nmvc} [\boldsymbol{\mu}_{nm}^{vc} d_n^v c_m^c + (\boldsymbol{\mu}_{nm}^{vc})^* c_m^{c+} d_n^{v+}], \end{aligned} \tag{9}$$

where $\mathbf{P}$ is the total optical interband polarization, which is given by summing over all microscopic polarizations $\boldsymbol{\mu}_{nm}^{vc} d_n^v c_m^c$ and $\boldsymbol{\mu}$ is the dipole matrix element for the optical transition between the valence and conduction bands. Since the nonlinear optical response depends significantly on the polarization directions of the incident pulses [8,9,17,21], the vector character of $\mathbf{E}$, $\boldsymbol{\mu}$, and $\mathbf{P}$ is important and thus is included here.

Using the total Hamiltonian H and the Heisenberg equation, one obtains the equation of motion of the interband coherence $p_{12}^{v_1c_2} = \langle d_1^{v_1} c_2^{c_2} \rangle$. Due to the many-particle Coulomb interaction the equations for expectation values of two operators, are coupled to four operator correlation functions [18,19], which is just the beginning of the infinite many-body hierarchy.

Considering optical excitation with weak intensities allows us to restrict the theoretical description to third order in the optical field. Furthermore, dephasing processes due to scattering with other quasiparticles are neglected. These two assumptions define the coherent $\chi^{(3)}$-limit. In this limit the electron and hole populations and coherences do not have to be treated as independent variables but can be expressed as [18,19]

$$f_{12}^{c_1c_2} = \langle {c_1^{c_1}}^{+} c_2^{c_2} \rangle = \sum_{av_a} p_{a2}^{v_a c_2} (p_{a1}^{v_a c_1})^* , \tag{10}$$

$$f_{12}^{v_1v_2} = \langle {d_1^{v_1}}^{+} d_2^{v_2} \rangle = \sum_{ac_a} p_{2a}^{v_2 c_a} (p_{1a}^{v_1 c_a})^* . \tag{11}$$

Similarly, the four-point terms appearing in the direct evaluations of the equation of motion for p can be written as [18,19]

$$\langle {d_a^{v_a}}^{+} d_1^{v_1} d_a^{v_a} c_2^{c_2} \rangle = \sum_{bc_b} \langle d_1^{v_1} c_b^{c_b} d_a^{v_a} c_2^{c_2} \rangle (p_{ab}^{v_a c_b})^* . \tag{12}$$

Applying these conservation laws the nonlinear optical response can be expressed using just two transition-type quantities which describe the coherences between a single and two interacting electron-hole pairs.

It is convenient to remove the uncorrelated parts from the four-particle correlation function and to define [9,21]

$$\bar{B}_{1234}^{v_1cvc_2} = \langle d_1^{v_1} c_2^c d_3^v c_4^{c_2} \rangle - p_{12}^{v_1 c} p_{34}^{vc_2} + p_{14}^{v_1 c_2} p_{32}^{vc} . \tag{13}$$

This procedure results in closed equations of motion for the single-exciton amplitude p_{12}^{vc} and the (reduced) two-exciton amplitude $\bar{B}_{1234}^{v_1cvc_2}$. The equation of motion for the single-exciton amplitude p and the two-exciton amplitude $\bar{B}$ read:

$$\begin{aligned} -\mathrm{i}\partial_t p_{12}^{vc} = & -\sum_j T_{2j}^c p_{1j}^{vc} - \sum_i T_{i1}^v p_{i2}^{vc} + V_{12} p_{12}^{vc} \\ & + \mathbf{E}(t) \cdot [(\boldsymbol{\mu}_{12}^{vc})^* - \sum_{abv'c'} ((\boldsymbol{\mu}_{1b}^{vc'})^* (p_{ab}^{v'c'})^* p_{a2}^{v'c} \\ & + (\boldsymbol{\mu}_{b2}^{v'c})^* (p_{ba}^{v'c'})^* p_{1a}^{vc'})] \\ & + \sum_{abv'c'} (V_{a2} - V_{a1} - V_{b2} + V_{b1}) [(p_{ba}^{v'c'})^* p_{b2}^{v'c} p_{1a}^{vc'} \\ & - (p_{ba}^{v'c'})^* p_{ba}^{v'c'} p_{12}^{vc} - (p_{ba}^{v'c'})^* \bar{B}_{ba12}^{v'c'vc}] , \end{aligned} \tag{14}$$

and

$$\begin{aligned} -\mathrm{i}\partial_t \bar{B}_{ba12}^{v'c'vc} = & -\sum_i (T_{2i}^c \bar{B}_{ba1i}^{v'c'vc} + T_{i1}^v \bar{B}_{bai2}^{v'c'vc} \\ & + T_{ai}^c \bar{B}_{bi12}^{v'c'vc} + T_{ib}^v \bar{B}_{ia12}^{v'c'vc}) \\ & + (V_{ba} + V_{b2} + V_{1a} + V_{12} - V_{b1} - V_{a2}) \bar{B}_{ba12}^{v'c'vc} \\ & - (V_{ba} + V_{12} - V_{b1} - V_{a2}) p_{1a}^{vc'} p_{b2}^{v'c} \\ & + (V_{1a} + V_{b2} - V_{b1} - V_{a2}) p_{ba}^{v'c'} p_{12}^{vc} . \end{aligned} \tag{15}$$

The first line in equation (14) defines the homogeneous part of the equation of motion for p, which includes the electronic energies and couplings (T) and the electron-hole Coulomb attraction (V_{12}). The next lines describe different types of driving terms. In addition to the linear source term given by the external field times the dipole transition matrix element, $\mathbf{E}(t) \cdot \boldsymbol{\mu}^*$, in the coherent $\chi^{(3)}$-limit there are the optical nonlinearities arising from three processes. The first one is the Pauli blocking, $\mathbf{E}(t) \cdot \boldsymbol{\mu}^* p^* p$, which is the only nonlinearity present in the optical Bloch equations where Coulomb interactions are neglected. The other two nonlinearities are induced by the many-body Coulomb interaction. They include the first-order Coulomb contribution (Vp^*pp) and the correlation contribution ($Vp^*\bar{B}$) [8,9,21], which involves two-exciton resonances.

The first three lines in equation (15) constitute the homogeneous part of the equation of motion for $\bar{B}$, which includes the electronic energies and couplings (T) as well as the six possible Coulomb-interactions between the two electrons and the two holes. The eigenmodes of $\bar{B}$ correspond to correlated complexes of two electrons and two holes, *i.e.* two-exciton states, including both bound biexcitonic and unbound continuum states. The last two lines in equation (15) represent the inhomogeneities. Since the uncorrelated contributions have been removed from $\bar{B}$ it is purely driven by sources which are proportional to the many-body interaction V [9,21], *i.e.* by terms proportional to Vpp.

The total interband polarization $\mathbf{P}$ is obtained from the sum

$$\mathbf{P} = \sum_{nmvc} \boldsymbol{\mu}_{nm}^{vc} p_{nm}^{vc} . \tag{16}$$

Equations (14) and (15) fully determine the interband polarization $\mathbf{P}$ within the coherent $\chi^{(3)}$-limit [8,9,18,19,21], also in the presence of disorder [17]. They have been used to analyze two-pulse experiments like pump-probe [8–11] and four-wave-mixing [17] spectroscopy. Alternatively, this set of equations for p and $\bar{B}$ can also be derived in k-space. For a spatially homogeneous system such equations have been presented in reference [21].

2.3 Model system

We use a regularized Coulomb-interaction potential to avoid the divergence of the exciton binding energy in one

dimension,

$$V_{nm} = U_0 \frac{d}{\frac{Nd}{\pi}\sin[\frac{\pi}{N}|n-m|] + a_0}\,. \tag{17}$$

Here Nd is the circumference of the ring and U_0 and a_0 are parameters characterizing the strength of the interaction and its spatial variation, respectively. The sin function in the denominator of equation (17) is needed to describe the distance between sites n and m on the ring. For quantum wires it has been shown that with a properly chosen a_0, which depends on the wire radius, such a regularized Coulomb potential is well suited to describe exciton and biexciton energies [22].

Concerning the band structure we consider two valence and conduction bands, respectively. For the valence bands we include the two energetically degenerate heavy-hole bands. These are characterized by the states $|-3/2h\rangle$ and $|3/2h\rangle$, respectively. The two energetically degenerate conduction bands are $|-1/2e\rangle$ and $|1/2e\rangle$. The light fields are assumed to propagate perpendicular to the system extension in the z-direction. We use the usual dipole matrix elements [9,21]:

$$\begin{aligned}
\boldsymbol{\mu}^{11}_{nm} &= \delta_{nm}\mu_0\boldsymbol{\sigma}^{+} = \delta_{nm}\frac{\mu_o}{\sqrt{2}}\begin{pmatrix}1\\ \mathrm{i}\end{pmatrix},\\
\boldsymbol{\mu}^{12}_{nm} &= \boldsymbol{\mu}^{21}_{nm} = 0,\\
\boldsymbol{\mu}^{22}_{nm} &= \delta_{nm}\mu_0\boldsymbol{\sigma}^{-} = \delta_{nm}\frac{\mu_o}{\sqrt{2}}\begin{pmatrix}1\\ -\mathrm{i}\end{pmatrix},
\end{aligned} \tag{18}$$

where μ_0 is the modulus of the matrix element for the heavy-hole transition. Consistent with the tight-binding description the optical transitions are taken as diagonal in the site index. Due to these selection rules (Eq. (18)), we have two separate subspaces of states, which are optically isolated but coupled by the many-body Coulomb interaction.

In our subsequent numerical evaluations we use $J_c = 28.05$ meV and $J_v = 4.95$ meV. The corresponding effective masses can be evaluated from $m^* = \hbar^2/2Jd^2$, where d is the distance between neighboring sites [13]. This choice of tight-binding couplings models a direct-gap GaAs type semiconductor in the absence of disorder. The ratio of the conduction and valence band couplings J_c/J_v matches the ratio of the inverse ratio of the effective conduction and valence band masses $(m^*_c/m^*_v)^{-1}$ for GaAs parameters. For the Coulomb interaction we use $U_0 = 15$ meV (in two sets of calculations we use $U_0 = 0$ and $U_0 = 22.5$ meV) and $a_0/d = 0.5$. This choice of parameters results in exciton binding energies of a reasonable magnitude. The number of sites is taken to be $N = 10$ (in one set of calculations we use $N = 20$). These parameters have to be varied, if one wants to model nanorings with a certain geometry made of a particular material system. The values used here were chosen in order to clearly demonstrate how a magnetic field qualitatively influences single- and two-exciton states.

3 Numerical results

3.1 Ordered system

We start by investigating the influence of the enclosed magnetic flux on the excitonic line in the linear absorption spectrum. Since all changes are periodic with $\cos(2\pi\Phi/\Phi_0)$ [6,7] we limit our investigations to $0 \leq \Phi/\Phi_0 \leq 0.5$. Figure 1a displays the excitonic linear absorption for different flux ratios $\mathcal{R} = \Phi/\Phi_0$. Note that the zero of the energy scale corresponds to the lowest optical transition without Coulomb interaction and without magnetic field ($\mathcal{R} = 0$, see Fig. 1b), *i.e.* to the band gap energy E_g. Thus for $\mathcal{R} = 0$ we have the exciton line at $E_X = -11.86$ meV which directly corresponds to an exciton binding energy of 11.86 meV. With increasing flux, Figure 1a shows that the exciton line shifts towards higher energies and that the oscillator strength is increasing [7]. The variation of the exciton energy with flux closely follows the $\cos(2\pi\Phi/\Phi_0)$-law obtained in references [6,7].

A larger excitonic oscillator strength implies that the part of the exciton wavefunction describing the relative motion of the electron and hole must have a higher value at the origin, *i.e.* at $r_e = r_h$ [20]. This corresponds to an increased exciton binding energy. Since the exciton binding energy is defined with respect to the lowest optical transition of the same system without Coulomb interaction, E_g, we have to calculate also $E_g(\mathcal{R})$, see Figure 1b.

Without magnetic field the lowest optical transition corresponds in k-space to a transition between the $k = 0$ electron and hole states. The phase factor introduced by the magnetic field in real space, see Section 2.1, results in an effective shift of the allowed values of the wavevectors in k-space. Therefore $E_g(\mathcal{R})$ increases monotonically when the enclosed flux increases from $\Phi = 0$ to $\Phi = 0.5\Phi_0$, see Figure 1b. The second allowed interband transition, which is twofold degenerate without magnetic field corresponding to $k = 2\pi/Nd$ and $k = -2\pi/Nd$, splits into two lines with increasing magnetic field. Due to the magnetic-field-induced shift of the k-values, one of these lines increases and one decreases in energy. At $\Phi = 0.5\Phi_0$ the lowest transition is twofold degenerate corresponding to $k = \pi/Nd$ and $k = -\pi/Nd$.

As shown in Figure 1c, $-E_X(\mathcal{R})$ is cos-like and decreases slightly, whereas $E_g(\mathcal{R})$ increases quadratically since the cos tight-binding dispersion in the vicinity of the band-gap is quadratic. Due to the fact that $E_g(\mathcal{R})$ increases more strongly than $-E_X(\mathcal{R})$ decreases, the exciton binding energy defined as $\Delta E_X(\mathcal{R}) = E_g(\mathcal{R}) - E_X(\mathcal{R})$ increases as function of $\mathcal{R}$. Thus in agreement with the increase in oscillator strength shown in Figure 1a, we find that also the exciton binding energy increases when going from $\mathcal{R} = 0$ to $\mathcal{R} = 0.5$.

An interesting qualitative analogy exists with the shift of the excitonic absorption in a superlattice biased by an ac electric field [23]. As the magnetic field considered here, also the ac electric field used in reference [23] changes the single-particle dispersion and moves due to dynamical localization [24–26] the lowest optical transition without

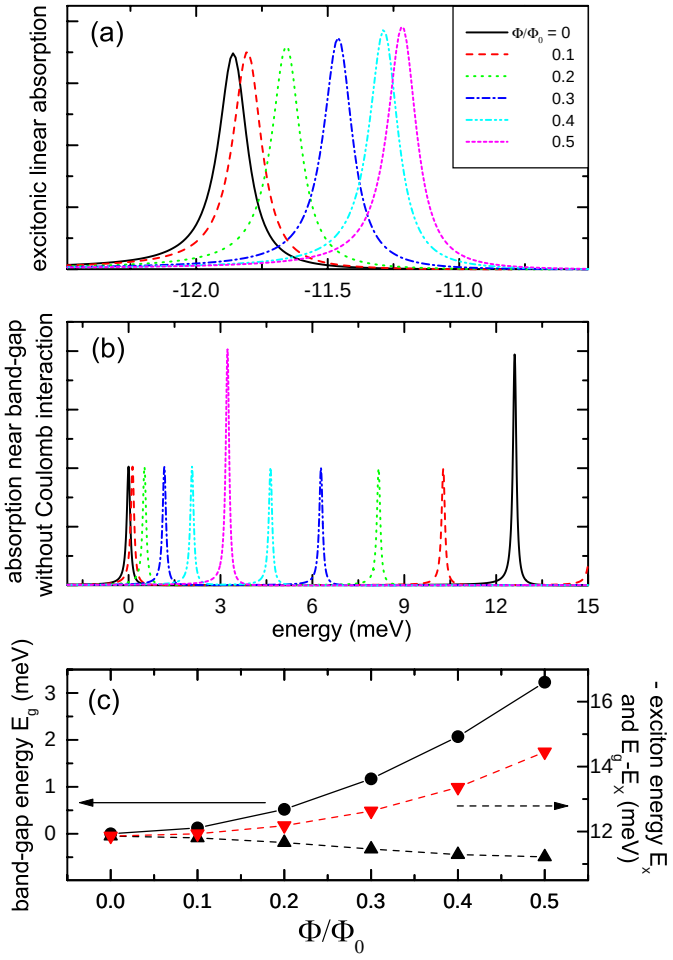

Fig. 1. (a) Excitonic linear optical absorption spectra and (b) interband absorption without Coulomb interaction close to the band gap for various magnetic fields corresponding to $\mathcal{R} = \Phi/\Phi_0 = 0$, 0.1, 0.2, 0.3, 0.4, and 0.5. In both cases Lorentzian homogeneous broadening is introduced by inserting a decay time of $T_2 = 10$ ps into equation (14). (c) Band-gap energy E_g (circles) and the negative of the exciton energy $-E_X$ (triangles up), as well as difference between between both $E_g - E_X$ (triangles down). The symbols correspond to calculated vales, the lines are guides for the eye.

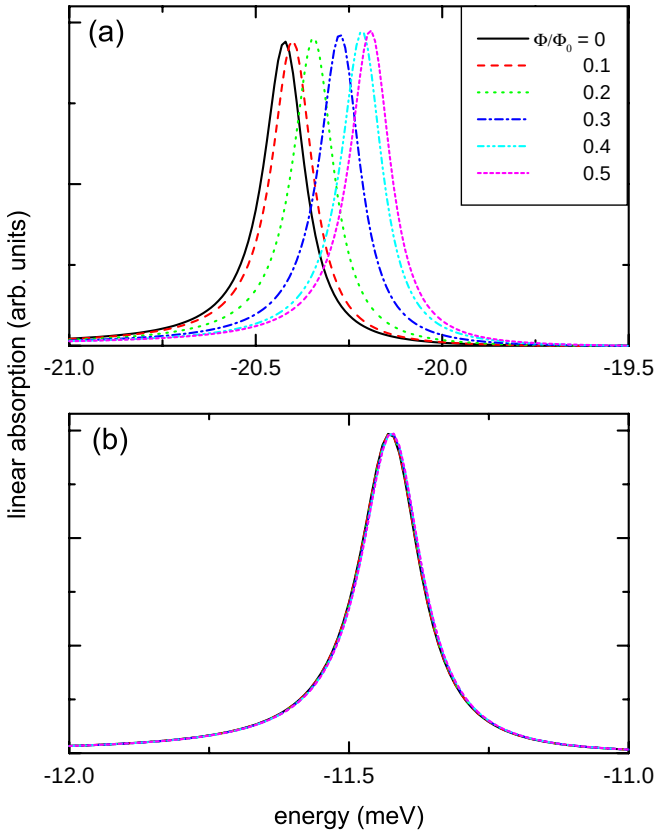

Fig. 2. Excitonic linear optical absorption spectra for various magnetic fields corresponding to $\mathcal{R} = \Phi/\Phi_0 = 0$, 0.1, 0.2, 0.3, 0.4, and 0.5. (a) For an increased Coulomb interaction of $U_0 = 22.5$ meV and (b) for an increased system size of $N = 20$. In both cases Lorentzian homogeneous broadening is introduced by inserting a decay time of $T_2 = 10$ ps into equation (14).

Coulomb interaction towards higher values. Since this dynamical localization is accompanied by a change of the effective dimension of the exciton from 3 to close to 2, the binding energy of the exciton increases when the ac electric field is applied. Thus, as found in reference [23], we see also here simultaneously a blue shift and an increase of the oscillator strength and binding energy of the exciton (Fig. 1a).

As the analysis of references [6,7] has shown, the change of the exciton energy due to the Aharanov-Bohm effect does occur only in mesoscopic systems. Since the effect relies on the finite probability of the electron and hole forming the exciton to tunnel around the ring, the exciton Bohr radius needs to be comparable to the diameter of the ring. If we increase the Coulomb interaction by a factor of 1.5, *i.e.* we use $U_0 = 22.5$ meV, then the exciton is more strongly bound and the Bohr radius decreases. Concomitantly, the shift of the exciton energy in the range $\mathcal{R} = 0$ to $\mathcal{R} = 0.5$ is reduced in Figure 2a as compared to Figure 1a. Another clear demonstration of the mesoscopic nature of the excitonic Aharanov-Bohm effect is given in Figure 2b, where it is shown that when using the original parameters, *i.e.* $U_0 = 15$ meV, the effect has almost completely disappeared for a doubled number of sites $N = 20$ corresponding to a doubled diameter of the ring.

The nonlinear optical response of the ring is analyzed by calculating the differential absorption as obtained in pump-probe spectroscopy performed with counter-clockwise polarized pulses ($\sigma^+\sigma^-$). In this geometry the differential absorption spectra of an ordered system are purely induced by many-body correlations as long as only heavy-hole and no light-hole transitions are relevant [8–11]. This is due to the fact that the two degenerate optically allowed heavy-hole excitons that can be excited with σ^+ and σ^- polarized light do not share a common state, see Section 2.3.

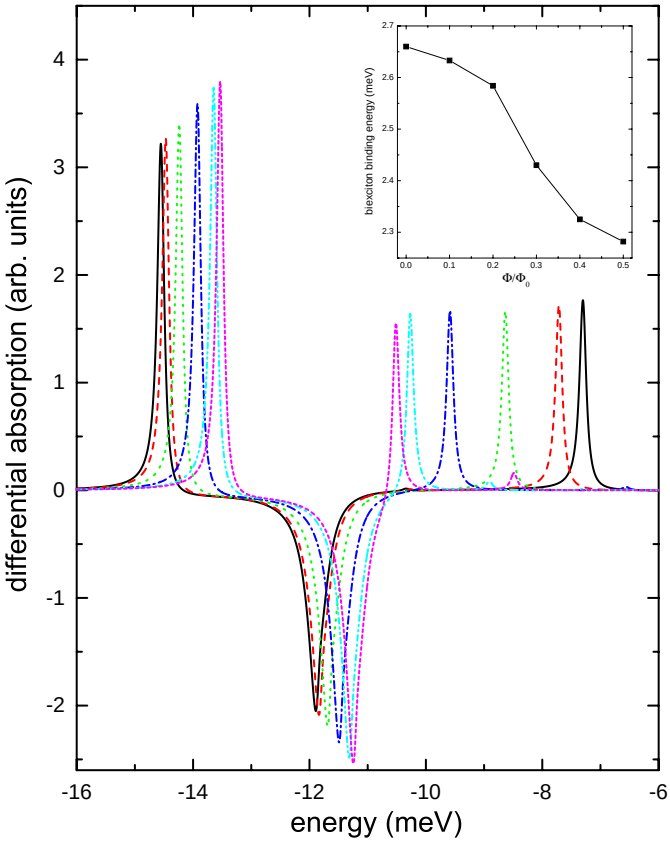

Fig. 3. Differential absorption spectra using a σ^+ polarized pump and a σ^- polarized probe pulse for various magnetic fields corresponding to $\mathcal{R} = \Phi/\Phi_0 = 0$, 0.1, 0.2, 0.3, 0.4, and 0.5. The pump pulse arrives 2 ps before the probe, its duration is 1.18 ps (FWHM of pulse intensity), and it is spectrally tuned to the exciton resonance for each value of the field. A Lorentzian homogeneous broadening is introduced by inserting a decay time of $T_2 = 10$ ps into equation (14). No broadening is used in equation (15) in order to obtain spectrally narrow two-exciton lines. The inset shows the flux dependence of the biexciton binding energy obtained as $\Delta E_{BX} = 2E_X - E_{BX}$.

The spectra displayed in Figure 3 show negative contributions at the exciton energy which correspond to the pump-induced bleaching of the exciton transition [8,9]. Positive induced absorption appears spectrally below and above the exciton due to transitions to bound and unbound two-excitons, respectively. As the exciton, also the spectral position of the exciton to bound biexciton transition, that appears at $E_{BX} - E_X$, shifts towards higher energies when $\mathcal{R}$ increases from 0 to 0.5. The fact that the exciton to bound biexciton transition shifts more strongly with $\mathcal{R}$ than the exciton line, corresponds to a *decrease* of the biexciton binding energy $\Delta E_{BX} = 2E_X - E_{BX}$, see inset of Figure 3. So comparing the cases $\mathcal{R} = 0$ with $\mathcal{R} = 0.5$ we find that the increase of the exciton binding energy is accompanied by a decrease of the biexciton binding energy of about 15%. This can be understood to be due to the weaker interaction among the more tightly bound excitons. If the excitons would be very strongly bound, *i.e.* if the electron and hole would be confined to the same site as in a Frenkel exciton, then the biexciton binding energy would vanish and only unbound two-excitons would appear in the spectra [27,28]. Thus with the magnetic-field-induced stronger exciton binding we go from an extended Wannier towards a more tightly bound Frenkel exciton. A decrease of the biexciton binding energy comparing the cases $\mathcal{R} = 0$ with $\mathcal{R} = 0.5$ has been observed for all parameters that have been investigated, *i.e.* this effect seems to be robust and especially survives for larger as well as weaker Coulomb interaction (not shown in figure).

As clearly shown in Figure 3, the magnetic field shifts not only the resonances of bound biexcitons to higher energies, but also introduces an even stronger red shift of the lowest unbound two-exciton resonance. *I.e.* the stronger binding of the excitons introduces a weaker repulsive interaction among them, which is consistent with the explanation given above.

3.2 Disordered system

Disorder is introduced as a site dependence of the electron and hole energies, *i.e.* $T^c_{nn} = E_g/2 + \delta\epsilon^c_n$ and $T^v_{nn} = E_g/2 + \delta\epsilon^v_n$. $\delta\epsilon^c_n$ is taken randomly from a Gaussian distribution function $\exp(-(\delta\epsilon^c)^2/2\sigma_c^2)$, where σ_c characterizes the energetic scale of the disorder. We assume that the disorder for electrons and holes is correlated, which is often the case in semiconductor nanostructures. Therefore we take $\delta\epsilon^v_n = (J_v/J_c)\delta\epsilon^c_n = (m^*_c/m^*_v)\delta\epsilon^c_n$, *i.e.* we weight the energetic variations inversely with the masses.

Figure 4a displays the excitonic linear optical absorption spectra for $\mathcal{R} = 0$ (solid) and $\mathcal{R} = 0.5$ (dashed) for the ordered system. The spectra displayed in Figures 4b and c were calculated by averaging over 10 000 disorder realizations (corresponding to a measurement on an ensemble of 10 000 rings) using $\sigma_c = 2$ meV and 4 meV, respectively. They show some fluctuations due to the finite number of disorder realizations and a much broader and red shifted exciton absorption than the spectra for the ordered system. This can be understood to be the result of the disorder-induced inhomogeneous broadening of the excitonic transition energy. Even for these quite broad spectra which are characterized by an inhomogeneous linewidth that exceeds the magnetic-field-induced shift of the exciton line, one can still see an effect of the magnetic field. Thus the shift of the exciton line due to the magnetic field seems not to be destroyed by energetic disorder on the scale considered here and even survives the inhomogeneous broadening.

Even more interesting than the disorder-induced inhomogeneous broadening is the question of how the disorder influences the relative motion of the electron-hole pair forming the exciton. Note that in order to show any Aharanov-Bohm effect the relative motion of the exciton needs to extend over the entire ring, see Section 3.1. This condition will not be fulfilled if the disorder is strong enough to localize the relative motion to a small portion of the ring. In order to address this problem

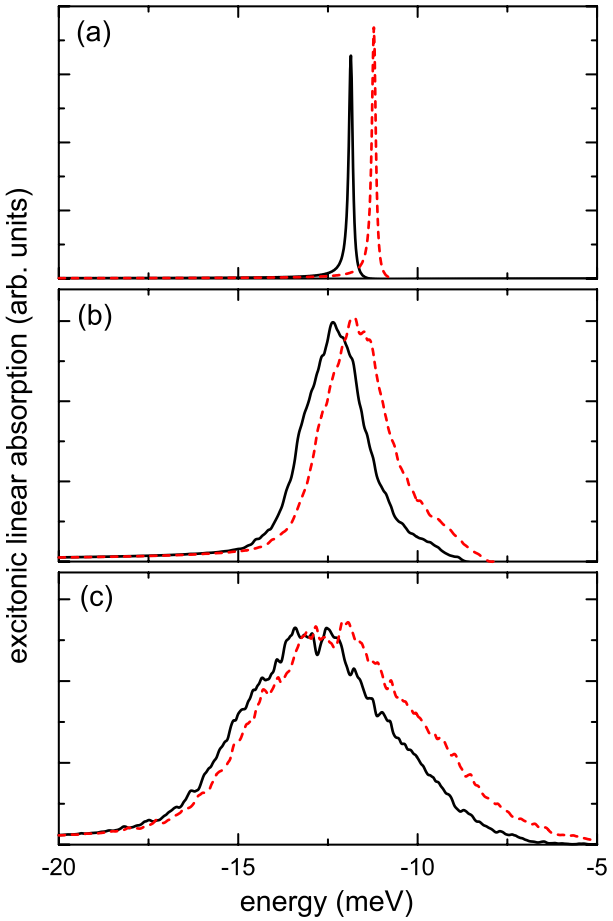

Fig. 4. Excitonic linear optical absorption spectra for magnetic fields corresponding to $\mathcal{R} = \Phi/\Phi_0 = 0$ (solid) and 0.5 (dashed). (a) Without disorder, (b) with disorder described by $\sigma^c = 2$ meV, and (c) for $\sigma^c = 4$ meV. Lorentzian homogeneous broadening is introduced by inserting a decay time of $T_2 = 10$ ps into equation (14). For (b) and (c) the spectra have been averaged over 10 000 disorder realizations.

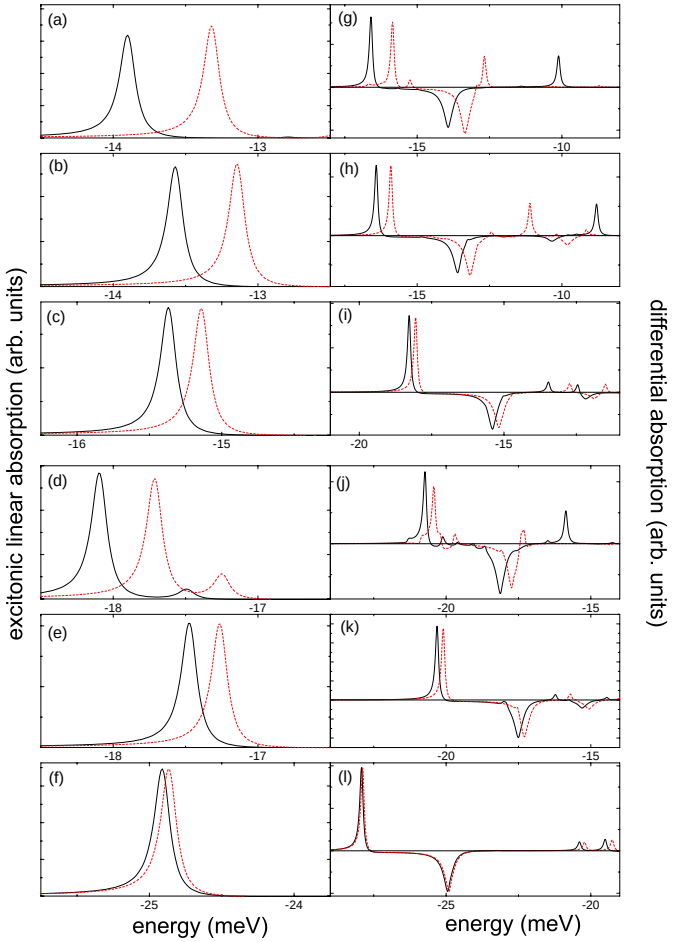

Fig. 5. Left panels: Excitonic linear optical absorption spectra for magnetic fields corresponding to $\mathcal{R} = \Phi/\Phi_0 = 0$ (solid) and 0.5 (dashed). (a–c) three individual disorder realizations with $\sigma^c = 4$ meV and (d–f) the same realizations for $\sigma^c = 10$ meV. Right panels: Differential absorption spectra using a σ^+ polarized pump and a σ^- polarized probe pulse for $\mathcal{R} = \Phi/\Phi_0 = 0$ (solid) and 0.5 (dashed). (g–i) for the same disorder realizations as (a–c) and (j–l) for the same disorder realizations as (d–e). The pump pulse arrives 2 ps before the probe, its duration is 1.18 ps (FWHM of pulse intensity), and it is spectrally tuned to the exciton resonance for each value of the field. A Lorentzian homogeneous broadening is introduced by inserting a decay time of $T_2 = 10$ ps into equation (14). No broadening is used in equation (15) in order to obtain spectrally narrow two-exciton lines. Zero differential absorption is indicated by the horizontal line.

we investigate linear and nonlinear absorption spectra for individual disorder realizations.

For $\sigma^c = 4$ meV the magnetic-field-induced shift of the exciton energy is still present, see Figures 5a–c, however, it is smaller than without disorder (*cp.* Fig. 1a) and its precise value depends on the disorder realization. Whereas for one realization, Figure 5a, there is still some observable increase of the oscillator strength of the exciton, it gets much smaller for another realization, Figure 5b, and is absent in the third case, Figure 5c. Consequently, only for one disorder realization (Fig. 5a) the magnetic field does still significantly influence the relative motion of the exciton. This results in a clear reduction of the interaction among excitons as demonstrated by the corresponding nonlinear pump-probe spectrum shown in Figure 5g. As in the ordered case, the energy difference between the exciton and the bound biexciton as well as between the exciton and the lowest unbound two-exciton state is smaller for $\mathcal{R} = 0.5$ than for $\mathcal{R} = 0$. In Figures 5h and i on the other hand, the biexciton binding energy is unaffected by the magnetic field. One can still see some reduction of the energy difference between the exciton and the lowest unbound two-exciton state in Figure 5h. Additionally, the disorder is responsible for the weak additional lines appearing the in pump-probe spectra.

Even when the disorder is increased to $\sigma^c = 10$ meV (note that this value is close to the exciton binding energy) all three realizations still show some reduced shift of the exciton energy, see Figures 5d–f. The weak absorption line above the lowest exciton appearing in Figure 5d is induced by the disorder. For $\sigma^c = 10$ meV, however,

no realization shows any increase of the exciton oscillator strength. Consequently, also the biexciton binding energy is unaffected by the magnetic field, see Figures 5j–l.

4 Summary

Linear and nonlinear optical properties of interband transitions in semiconductor nanorings in the presence of penetrating magnetic fields have been investigated. As predicted in references [6,7], the spectral position of the exciton line in the linear absorption spectra as well as its oscillator strength change periodically with the magnetic flux Φ enclosed by the ring. The period of these oscillations is given by the flux quantum $\Phi_0 = hc/e$.

By analyzing nonlinear pump-probe spectra performed with counter-clockwise polarized pulses it is demonstrated that the magnetic field modifies the Coulombic many-particle correlations. The stronger exciton binding induced by the magnetic field leads to a weaker interaction among the excitons. In particular, the binding energy of the bound biexciton changes as function of Φ and is smaller for $\Phi/\Phi_0 = 0.5$ than without magnetic field, whereas the exciton binding energy increases. Our findings demonstrate that the Aharanov-Bohm effect leads to a characteristic influence on quasiparticles like excitons and biexcitons. We believe that it should be possible to experimentally investigate such effects using optical interband spectroscopy performed on high-quality semiconductor nanorings. To be able to observe Aharanov-Bohm effects the diameter of the nanorings should not be much bigger than the exciton Bohr radius [7], and their width must be much smaller.

Since semiconductor nanostructures are typically not fully ordered systems, we have investigated the influence of disorder on the linear and nonlinear optical properties of semiconductor rings. It is demonstrated that in an ensemble averaged measurement the magnetic-field-induced shift of the exciton line survives even when the disorder-induced inhomogeneous broadening of the spectral lines is larger than the shift. By studying single rings it is demonstrated that for intermediate disorder the strength of the Aharanov-Bohm effects for the excitons and biexcitons may depend on the disorder realization. When the energetic disorder is on the scale of the exciton binding energy the influence of the magnetic field on the relative motion of the exciton is suppressed.

We acknowledge stimulating discussions with R.A. Römer and M.E. Raikh. This work is supported by the Deutsche Forschungsgemeinschaft (DFG) through the Sonderforschungsbereich 383, the Leibniz program, the Max-Planck Research program of the Humboldt and Max-Planck societies, and by the John von Neumann Institut für Computing (NIC), Forschungszentrum Jülich, Germany, through grants for extended CPU time on their supercomputer systems.

References

1. D. Mailly, C. Chapelier, A. Benoit, Phys. Rev. Lett. **70**, 2020 (1993).
2. A.F. Morpurgo, J.P. Heida, T.M. Klawijk, B.J. Wees, G. Borghs, Phys. Rev. Lett. **80**, 1050 (1998).
3. A. Lorke, R.J. Luyken, A.O. Govorov, J.P. Kotthaus, J.M. Garcia, P.M. Petroff, Phys. Rev. Lett. **84**, 2223 (2000).
4. R.J. Warburton, C. Schäflein, D. Haft, F. Bickel, A. Lorke, K. Karrai, J.M. Garcia, W. Schoenfeld, P.M. Petroff, Nature **405**, 926 (2000).
5. H. Pettersson, R.J. Warburton, A. Lorke, K. Karrai, J.P. Kotthaus, J.M. Garcia, P.M. Petroff, Physica E **6**, 510 (2000).
6. A. Chaplik, Pis'ma Zh. Éksp. Teor. Fiz. **62**, 885 (1995) [JETP Lett. **62**, 900 (1995)].
7. R.A. Römer, M.E. Raikh, Phys. Rev. B **62**, 7045 (2000); phys. stat. sol. (b) **221**, 535 (2000).
8. C. Sieh, T. Meier, F. Jahnke, A. Knorr, S.W. Koch, P. Brick, M. Hübner, C. Ell, J. Prineas, G. Khitrova, H.M. Gibbs, Phys. Rev. Lett. **82**, 3112 (1999).
9. C. Sieh, T. Meier, A. Knorr, F. Jahnke, P. Thomas, S.W. Koch, Eur. Phys. J. B **11**, 407 (1999).
10. S.W. Koch, C. Sieh, T. Meier, F. Jahnke, A. Knorr, P. Brick, M. Hübner, C. Ell, J. Prineas, G. Khitrova, H.M. Gibbs, J. Lumin. **83/84**, 1 (1999).
11. T. Meier, S.W. Koch, M. Phillips, H. Wang, Phys. Rev. B **62**, 12605 (2000).
12. Y. Aharonov, D. Bohm, Phys. Rev. **115**, 485 (1959).
13. K. Maschke, T. Meier, P. Thomas, S.W. Koch, Eur. Phys. J. B **19**, 599 (2001).
14. N. Byers, C.N. Yang, Phys. Rev. Lett. **7**, 46 (1961).
15. F. Bloch, Phys. Rev. B **2**, 109 (1970).
16. M. Büttiker, Y. Imry, R. Landauer, Phys. Lett. A **96**, 365 (1983).
17. S. Weiser, T. Meier, J. Möbius, A. Euteneuer, E.J. Mayer, W. Stolz, M. Hofmann, W.W. Rühle, P. Thomas, S.W. Koch, Phys. Rev. B **61**, 13088 (2000).
18. V.M. Axt, A. Stahl, Z. Phys. B **93**, 195 (1994); *ibid.*, 205 (1994).
19. M. Lindberg, Y.Z. Hu, R. Binder, S.W. Koch, Phys. Rev. B **50**, 18060 (1994).
20. H. Haug, S.W. Koch, *Quantum Theory of the Optical and Electronic Properties of Semiconductors*, (World Scientific, Singapore, 1994).
21. W. Schäfer, D.S. Kim, J. Shah, T.C. Damen, J.E. Cunningham, K.W. Goossen, L.N. Pfeiffer, K. Köhler, Phys. Rev. B **53**, 16429 (1996).
22. L. Bányai, I. Galbraith, C. Ell, H. Haug, Phys. Rev. B **36**, 6099 (1987).
23. T. Meier, F. Rossi, P. Thomas, S.W. Koch, Phys. Rev. Lett. **75**, 2558 (1995).
24. D.H. Dunlap, V.M. Kenkre, Phys. Rev. B **34**, 3525 (1986).
25. M. Holthaus, Phys. Rev. Lett. **69**, 351 (1992).
26. T. Meier, G. von Plessen, P. Thomas, S.W. Koch, Phys. Rev. B **51**, 14490 (1995).
27. T. Meier, V. Chernyak, S. Mukamel, J. Phys. Chem. B **37**, 7332 (1997).
28. W.M. Zhang, T. Meier, V. Chernyak, S. Mukamel, J. Chem. Phys. **108**, 7763 (1998).